Silver-Based Self-Powered pH-Sensitive Pump and Sensor

Kayla Gentile, Subhabrata Maiti, Allison Brink, Bhargav Rallabandi,* Howard A. Stone,*
and Ayusman Sen*

ABSTRACT: Nonmechanical nano/microscale pumps that provide precise control over flow rate without the aid of an external power source and that are capable of turning on in response to specific analytes in solution are needed for the next generation of smart micro- and nanoscale devices. Herein, a self-powered chemically driven silver micropump is reported that is based on the two-step catalytic decomposition of hydrogen peroxide, H_2O_2. The pumping direction and speed can be controlled by modulating the solution pH, and modeling and theory allow for the kinetics of the reaction steps to be connected to the fluid velocity. In addition, by changing the pH dynamically using glucose oxidase (GOx)-catalyzed oxidation of glucose to gluconic acid, the direction of fluid pumping can be altered *in situ*, allowing for the design of a glucose sensor. This work underscores the versatility of catalytic pumps and their ability to function as sensors.
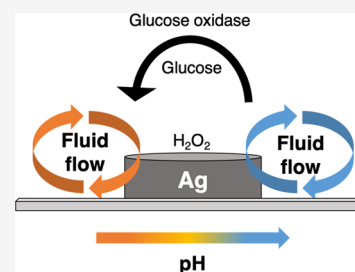
INTRODUCTION

Micropumps move small amounts of fluid and any suspended particles in a closed environment.[1−3] They are desirable for the fabrication of microfluidic devices, as they allow for chemically induced mixing, as well as the transport of molecules and colloidal particles to the desired locations.[4,5] Creating chemically powered, autonomous pumps is advantageous, as it allows for the development of systems that do not require external energy sources, such as electric or magnetic fields.[3,6,7] Such pumps facilitate the design of sensors that do not require bulky or expensive equipment and make possible drug delivery devices that are powered by chemicals found in the body.[6,8]

The discovery of catalytic micropumps[6] stemmed from the development of chemically powered nanomotors, small-scale devices that move by harvesting energy from chemical reactions.[3,9−11] Upon immobilization of a nanomotor on a surface and the introduction of the reactant, the generated mechanical force is transferred to the surrounding fluid resulting in fluid pumping.[3,6,7,12] Since the first discovery, the range of catalysts, fuels, and the mechanisms used to drive fluid motion have dramatically expanded.[3,6,9,13] The catalysts employed range from inorganic materials to enzymes. These pumps can be driven by a variety of mechanisms, such as self-electrophoresis, self-electroosmosis, self-diffusiophoresis, bubble propulsion, and buoyancy effects.[3,6,9,12−18]

Herein, we report a chemically powered silver micropump that is based on the decomposition of hydrogen peroxide, H_2O_2. Significantly, we are able to control the pumping direction and speed by modulating the solution pH and are able to connect reaction kinetics to the fluid velocity by using modeling and theory. Unlike previous metal-based catalytic pumps that operate through a self-electrophoretic mechanism,[10,11,18] the pumping in this system involves a buoyancy-driven mechanism similar to the previously studied enzyme micropumps.[6,12,17,19] However, unlike enzyme micropumps, this system is easier to fabricate and is much more robust. Experimentally, we were also able to change the pH dynamically using an enzyme, glucose oxidase (GOx). GOx decomposes neutral glucose to more acidic gluconic acid,[20] thereby altering the direction of fluid pumping *in situ* and creating a glucose sensor in the process. Our work clearly underscores the versatility of catalytic pumps and their ability to function as sensors.

EXPERIMENTAL SECTION

Fabricating Silver Patches. Tollen's reagent, aqueous [Ag-$(NH_3)_2$]$^+$, was used to make silver patches that were about 5 mm in diameter. To make the solution, a 500 μL solution of 100 mM AgNO$_3$ (Sigma-Aldrich) was prepared in nanopure water with a resistance of 18.2 MΩ. Ammonium hydroxide (28−30%, Sigma-Aldrich) was added in 4 μL increments until the solution turned clear (16−20 μL), and then 1 μL of sodium hydroxide (3 M, Alfa Aesar) was added. Glass slides (VWR) were cleaned with water and dried. To make the patches, 2 μL of Tollen's reagent was added to the slides. To reduce Tollen's reagent to metallic silver, 6 μL of 0.5 M D-(+)-glucose (Sigma-Aldrich) was added to the 2 μL of Tollen's reagent. The slides were allowed to dry for at least 1 h. Afterward, the slides were thoroughly rinsed with DI water and dried with air.

Preparation of Buffers and Glucose Oxidase. Acetate buffer (100 mM) was prepared at pH = 4 and 5 using acetic acid (glacial) (Sigma-Aldrich) and sodium acetate (Sigma-Aldrich). Nanopure water with a resistance of 18.2 MΩ was used, and the buffer was
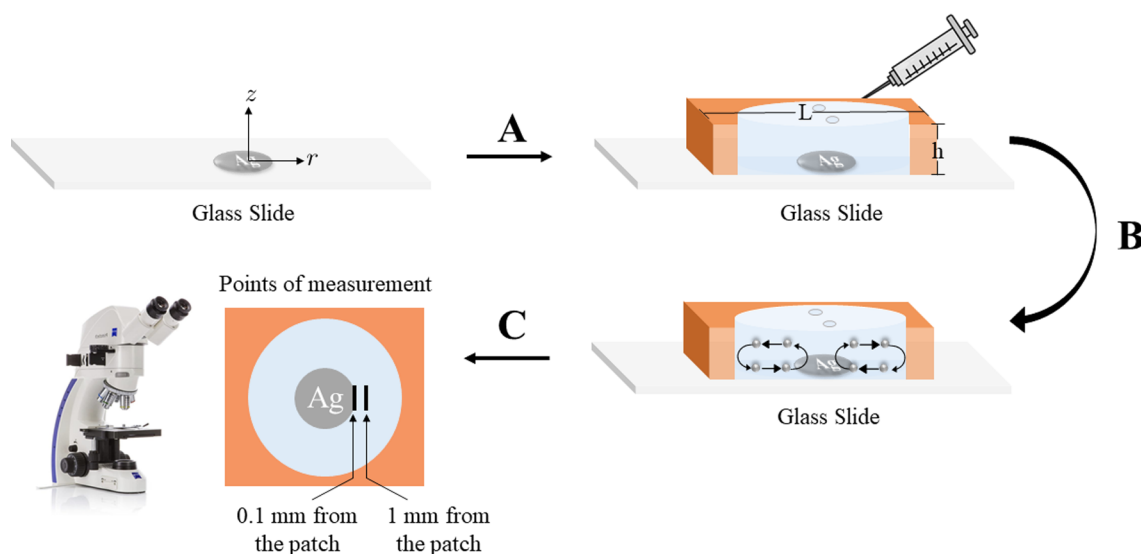
Figure 1. Schematic representation of the silver pump. A glass slide is functionalized with a silver patch (∼5 mm in diameter). (A) The patch is covered with a hybridization chamber, L = 20 mm and h = 0.9 mm. H_2O_2 solution (10 mM) with 2 μm diameter sulfate-functionalized tracer particles is added to the chamber. (B) Convective flow is induced. (C) Flows are monitored after 5 min with optical microscopy at 20× and at 150 μm above the surface, at either 0.1 or 1 mm away from the patch.

adjusted to pH = 4 and 5 by adjusting the ratio of acetic acid to sodium acetate. The pH was tested with a Thermo Scientific Orion Star pH meter. 2-(N-Morpholino)ethanesulfonic acid (MES) buffer (100 mM, pH 6 and 6.5) was prepared with MES (Sigma-Aldrich) using nanopure water with a resistance of 18.2 MΩ. The pH was adjusted to 6 and 6.5, respectively, using 3 M sodium hydroxide (Alfa Aesar) and tested using a Thermo Scientific Orion Star pH meter. (4-(2-Hydroxyethyl)-1-piperazineethanesulfonic acid) (HEPES, 100 mM) buffer (pH 7) was prepared with HEPES (Sigma-Aldrich), using nanopure water with a resistance of 18.2 MΩ. The pH was adjusted to 7 using 3 M sodium hydroxide (Alfa Aesar) and tested using a Thermo Scientific Orion Star pH meter. Borate buffer (100 mM) was prepared at pH = 8 and 9 using boric acid (Sigma-Aldrich) and sodium tetraborate decahydrate (Sigma-Aldrich). Nanopure water with a resistance of 18.2 MΩ was used, and the buffer was adjusted to pH = 8 and 9 using different ratios of boric acid to sodium tetrabrate. The pH was tested with a Thermo Scientific Orion Star pH meter. Glucose oxidase (1 mg mL^{-1}, 6.25 μM) from *Aspergillus niger* (Sigma-Aldrich), D-(+)-glucose (Sigma-Aldrich, 10 mM), and L-(−)-glucose (Sigma-Aldrich, 10 mM) were all prepared in nanopure water (resistance = 18.2 MΩ) and were used for the enzyme experiments.

Experimental Setup. Experiments were carried out using secure seal circular hybridization chambers (Electron Microscopy Sciences) with dimensions of 20 mm in length, 1.3 mm in height, and 0.9 mm (or 0.6 mm, depending on the experiment) in fluid depth. Sulfate-functionalized polystyrene particles (2 μm diameter, negatively charged, Polysciences Inc.) were used as tracer particles to monitor the fluid flow. Amine-functionalized polystyrene particles (2 μm diameter, positively charged, Polysciences Inc.) were used for determining the pumping mechanism. The tracer particles were introduced to the various buffer solutions to determine the pumping speed. Hydrogen peroxide (30%, VWR) was diluted and introduced (10 mM) to the solutions right before observation. The solutions were placed into the chamber using a needle (BD Precision Glide, 30G × 1/2, 0.3 mm × 13 mm) and syringe (Norm-ject Tuberlukin, 1 mL) and then sealed. The tracer particles were observed using an inverted microscope (Zeiss Axiovert 200 MAT) with a halogen lamp (12 V maximum, 100 W). Controls were done with no hydrogen peroxide to ensure that the flow was only due to the hydrogen peroxide and not due to heating from the lamp. A 20× objective (EC Epiplan-NEOFLUAR 20×/0.55 HD DIC ∞/0, Zeiss) was used at 3 V. The videos were recorded using a Flea 3 CCD camera (FL3-U3-

32S2C-CS, Point Grey) with a resolution of 1040 × 776 pixels at 60 frames per second (fps). Videos were recorded for 1800 frames at 60 fps at 0.1 mm and at 1 mm away from the patch after 5 min. Typically, videos were taken at 150 μm above the surface, unless otherwise specified. To measure the pumping velocity, 30 particles were analyzed using Tracker software (Cabrillo College) for 10 s.

Silver Ion Concentration Measurements. Silver patches were made in 20 mL scintillation glass vials (VWR). The same Tollen's reagent procedure was used, but 60 μL of Tollen's reagent solution was used with 180 μL of glucose. The vials were left to dry overnight and then rinsed thoroughly with DI water and dried in air. To measure the silver ion concentration in the vials, an ion-selective silver/sulfide electrode (Cole Parmer) was used. The electrode was attached to the Thermo Scientific Orion Star pH meter, and the voltage was measured. A calibration plot was first constructed with silver standards at 0.1, 1, 10, 100, and 1000 ppm (Figure S3). Using the given equation, the voltage was related to the experimental silver ion concentrations in ppm.

pH Measurements. pH measurements were carried out in 1.6 mL glass vials using a Thermo Scientific Orion Star pH meter. To better simulate the conditions in the experimental chamber, we used a micro pH probe attachment (Orion PerpHecT Ross Combination pH Micro Electrode) to measure the pH in smaller volumes (600 μL total). A silver patch (6 mm diameter) was made in the vial using Tollen's reagent chemistry (4 μL of Tollen's reagent solution was used with 12 μL of glucose). The vials were left to dry overnight and then rinsed thoroughly with DI water and dried in air. UV−vis measurements were carried out with a Thermo Scientific Evolution 220 UV−Visible Spectrophotometer. A quartz cuvette was used for measurement with 1 mL total volume, and the decomposition of hydrogen peroxide was followed at 240 nm.

■ RESULTS AND DISCUSSION

pH-Controlled Pumping. We used Tollen's reagent to functionalize a glass slide with a silver patch that was 5 mm in diameter.[21] Next, we fixed a hybridization chamber to the slide and added a solution of 10 mM H_2O_2 with 2 μm diameter tracer particles. The circular chamber (900 μm high, 20 mm diameter) was then sealed from the outside environment. We observed a spontaneous convective fluid flow near the patch, which was quantified using optical microscopy to follow the motion of the tracer particles. To obtain the flow velocities, we
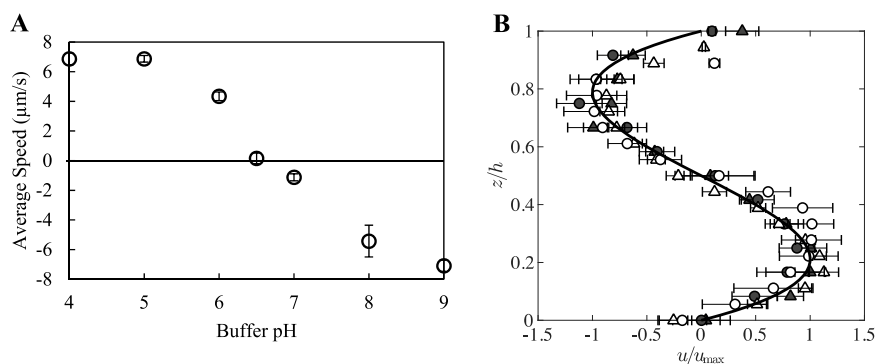
Figure 2. (A) Fluid flow velocities after 5 min, 0.1 mm away horizontally from the edge of the silver patch and at 150 μm above its surface for 10 mM buffers with different pH values. Positive fluid flow values indicate the fluid flow directed radially away from the silver patch. Negative fluid flow speeds indicate the fluid flow directed radially toward the silver patch. Fluid flows near 0 indicate Brownian motion (no mean motion was observed). See the Experimental Section for the buffers used. Error bars represent the standard deviation obtained from tracking 30 particles. The dimensions of the chamber are shown in Figure 1; the patch diameter was 5 mm. (B) Normalized horizontal velocity versus vertical position in the channel showing experimental measurements as symbols and the theoretical prediction of eq 1 as the solid curve. Symbols indicate velocities in a chamber of height 600 μm (filled) and 900 μm (open) measured at 0.1 mm radially outward from the edge of the patch (triangles) and 1 mm radially outward from the edge of the patch (circles).
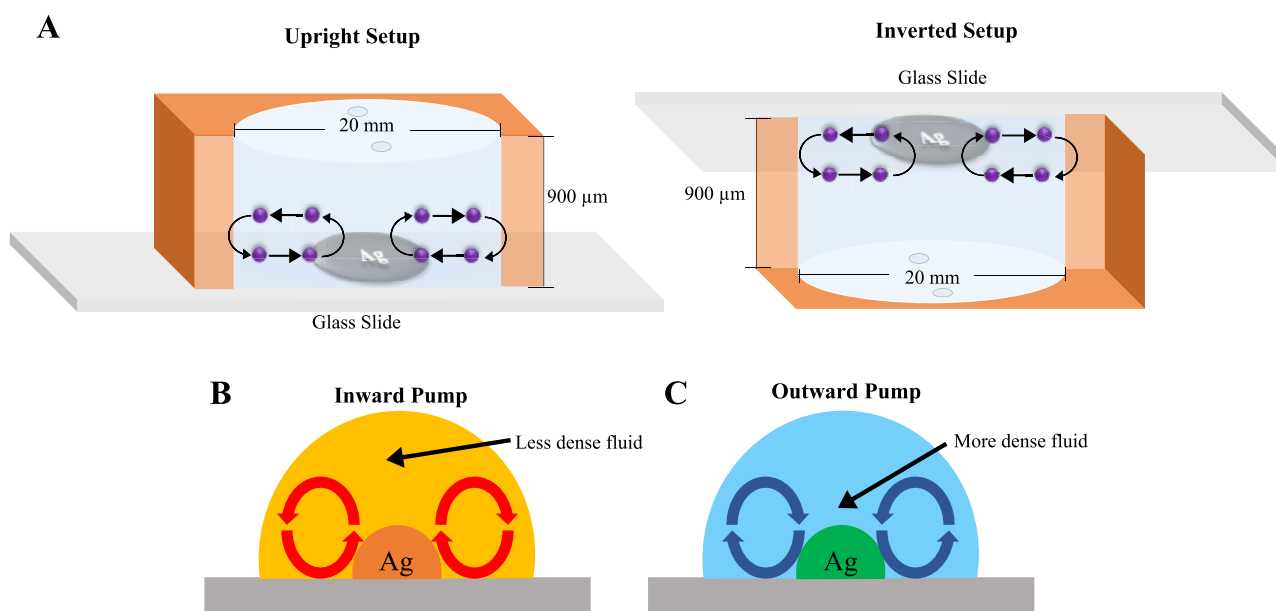
Figure 3. (A) Illustration of the upright and inverted setups and sketches of the observed fluid motion. The fluid flows toward the patch in the upright setup and the fluid flows away from the patch in the inverted setup. In a density-driven mechanism, the fluid flow next to the patch will change direction upon inversion. This is because less dense products will still rise upward, and more dense products will fall downwards. Because the setup is inverted, it appears that next to the patch, the flow is going in the opposite direction. (B, C) Illustration of a density-driven mechanism. (B) In the inward pump, the less dense fluid rises to the top and then falls back down and sinks along the bottom toward the silver patch. (C) In the outward pump, the more dense fluid sinks and slides away from the silver patch.

tracked 30 particles over 10 s using Tracker software. A schematic representation of the experiment is shown in Figure 1.

To examine the effect of pH on the pumping direction and speed, we studied the silver pumps in the presence of different buffers at pH values ranging from pH 4 to 9. With little or no buffer present, the fluid flow was directed radially toward the patch near the bottom of the chamber, which we will report as negative speeds, and away from the patch near the top of the chamber (Figure 1 and Video SV1). We refer to this flow orientation as "inward pumping" (the opposite orientation is referred to as "outward pumping", Video SV2). The speed and direction of fluid pumping at different solution pH values are shown in Figure 2A. Based on these results, we conclude that

higher pH favors inward pumping (negative speeds), while lower pH causes outward pumping (positive speeds), with a crossover at pH ~6.5 where the flow is negligible (Video SV3).

To quantify the spatial structure of the flow, we fixed the horizontal position at a distance from the edge of the patch and measured the horizontal velocity u at different vertical locations z (the bottom and top walls of the chamber are at $z = 0$ and $z = h$, respectively; Figure 1). These measurements were performed 0.1 and 1 mm away from the edge of the patch in channels of height 900 or 600 μm. For each experiment and each horizontal location, we extracted the maximum measured velocity across the channel height, which we denote by u_{max}. Figure 2B shows the normalized velocity profile u/u_{max} as a function of the normalized vertical coordinate z/h, plotted for
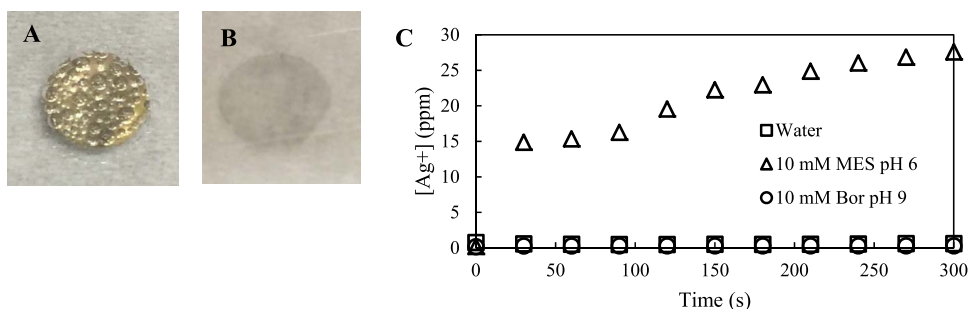
Figure 4. Images of the silver patch (5 mm diameter) after 10 min (A) in 10 mM borate buffer (pH 9) with 10 mM H_2O_2: bubbles were seen on the patch. (B) In 10 mM acetate buffer (pH 4) with 10 mM H_2O_2, no bubbles were seen on the patch and the patch is corroding due to the formation of silver ions. (C) Silver ion concentration (measured in ppm) for water (squares), 10 mM MES buffer (triangles), and 10 mM borate buffer (circles) during a reaction with 10 mM H_2O_2.

two different channel heights and two different horizontal distances from the edge of the patch. We obtain a universal distribution of velocities with a characteristic "S-shape" that shows clear antisymmetry about the mid-plane of the channel ($z = h/2$). The structure of the experimentally measured velocity distribution is in good agreement with theoretical predictions (described below) for buoyancy-driven flow (the solid curve in Figure 2B). Below, we provide further evidence for buoyancy being the main driving mechanism for the flow using both experiments and theory.

Pumping Mechanism. Previous work reported pumping by catalytic patches due to phoretic mechanisms, such as diffusiophoresis,[3,13] or density-driven mechanisms.[6,12,19] To determine the driving mechanism present in this work, we conducted a few key experiments to determine whether the mechanism is buoyancy-driven or phoretically driven. To test the importance of phoretic mechanisms, we seeded the fluid separately with positively charged tracers (2 μm diameter amine-functionalized polystyrene beads) and negatively charged tracers (2 μm diameter sulfate-functionalized polystyrene beads) and measured their motion. We observed that there was no change in the flow direction of the tracers and negligible changes in the tracer speed. This indicates that electrolyte diffusiophoresis is relatively unimportant in our system.[22−24] However, when we inverted the chamber, we found that the fluid flow direction next to the patch reversed, as indicated in Figure 3A. This implies that the mechanism is density-driven, as illustrated in Figure 3B,C.[12]

Guided by the experimental observations, we developed a reduced-order model for the fluid flow, including the effects of buoyancy, produced by local density differences between the reactants and products of chemical reactions catalyzed by the patch.[25−27] The vertical dimension of the device (typically 600−900 μm) is much smaller than its lateral dimensions (on the order of a few centimeters). Under this geometric condition and for a circular patch, we model the buoyancy-driven flow as axisymmetric and being driven by horizontal gradients of a height-averaged fluid density. We denote the local average density in the fluid in excess of its mean density ρ_0 by $\rho(r,t)$, where r measures the horizontal distances from the central axis of the patch (see Figure 1). We then find the fluid velocity to be[25,26]

$$u(r, z, t) = -\frac{g\nabla\rho}{6\mu}z(z-h)\left(z-\frac{h}{2}\right)$$
$$+ \frac{g}{24\mu}(\nabla^2\rho)z^2(z-h)^2 e_z \tag{1}$$

where μ is the viscosity of the fluid, e_z is the unit vector in the z direction, and $\nabla\rho = e_r\frac{\partial\rho}{\partial r}$ is the horizontal gradient of the height-averaged density and $\nabla^2\rho = \frac{1}{r}\frac{\partial}{\partial r}\left(r\frac{\partial\rho}{\partial r}\right)$. Thus, fluid flows in the direction of decreasing density in the bottom half of the channel and in the opposite direction in the top half of the channel, producing a convective flow pattern. Using eq 1, the maximum horizontal speed (maximized over the height of the chamber) of flow at a fixed horizontal location (r) is found to be

$$u_{max}(r, t) = \frac{gh^3|\nabla\rho|}{72\sqrt{3}\mu} \tag{2}$$

and occurs at $z \approx 0.21h$. The rescaled horizontal velocity u/u_{max} is a function only of the normalized vertical coordinate z/h and recovers the "S-curve", which is plotted in Figure 2B and is in good agreement with the experiments. These results further establish buoyancy, produced by local density differences in the fluid, as the dominant driver of flow in our system.

Chemical Origins of Pumping Mechanism. We investigated the source of the density differences driving the fluid flow as they relate to the underlying chemistry in the system. We considered the reaction steps involved in the silver-catalyzed decomposition of H_2O_2[28]

$$H_2O_2 + 2Ag^0 \rightleftharpoons 2Ag^+ + 2OH^- \tag{3a}$$

$$2Ag^+ + 2OH^- + H_2O_2 \rightleftharpoons 2Ag^0 + O_2 + 2H_2O \tag{3b}$$

$$2H_2O_2 \rightleftharpoons O_2 + 2H_2O \tag{3c}$$

The first step results in the formation of silver ions (Ag^+) and hydroxide (OH^-) ions. If the pH of the solution is low, OH^- is neutralized and the first reaction is driven toward the right-hand side according to Le Chatelier's principle. At the same time, the removal of OH^- by the acidic buffer attenuates the second reaction. The net result is a buildup of Ag^+, which is more dense than that of H_2O_2.[29] This results in a buoyancy-driven flow that is downward and then outward away from the silver patch (Figure 3C).

Conversely, if the pH of the solution is high, the first reaction occurs relatively slowly, while the second reaction is sped up. As a result, the steady-state concentration of Ag^+ remains low, while the second step rapidly produces O_2 and H_2O, which are less dense than H_2O_2.[29] This causes a flow that is inward toward the silver patch and then upward (Figure 3B).

The observations summarized in Figure 4 are consistent with the above hypothesis. In basic buffer, the overall reaction goes to completion and O_2 bubbles are seen (Figure 4A). On the other hand, O_2 evolution is not observed in an acidic buffer and the silver disk is corroded because of dissolution of Ag^+ (Figure 4B). Furthermore, as seen in Figure 4C, under acidic conditions (but not under neutral or basic conditions), the Ag^+ ion concentration in solution is significant.

The different chemical species in reactions 3a−c modify the local fluid density as they are produced, transported through the fluid, and then consumed. In particular, the fluid density depends on the local excess concentrations, relative to the bath (measured in mol m^{-3}), of H_2O_2 (c_2), Ag^+ (c_+), OH^- (c_-), and H_2O (c_w). These species have respective molar masses $M_2 \approx$ 0.034 kg mol^{-1}, $M_+ \approx$ 0.108 kg mol^{-1}, and $M_- \approx M_w \approx$ 0.018 kg mol^{-1}.[29] We neglect the density changes due to O_2 gas produced in reaction 3b, which remains adhered to the patch surface as gas bubbles (see Figure 4A). Stoichiometry lets us relate c_w and c_- to c_2 and c_+: If q mol m^{-3} of silver ions are consumed in reaction 3b for every 1 mol m^{-3} of silver ions produced in reaction 3a, then $c_2 = -(1 + q)/2$, $c_+ = c_- = 1 - q$, and $c_w = q$. Note that c_2 is negative since H_2O_2 is consumed in both reactions 3a and b, whereas c_+ is positive since the consumption of Ag^+ cannot exceed its production (i.e., $q \leq 1$). Then, the local height-averaged density excess (relative to the bath; measured in kg m^{-3}) is $\rho = M_+c_+ + M_-c_- + M_2c_2 + M_wc_w$, which can be simplified (after eliminating q) to

$$\rho = \left(M_+ + \frac{M_w}{2}\right)c_+ + (M_2 - M_w)c_2 \qquad (4)$$

The concentrations of H_2O_2 and Ag^+ depend on the reaction rates in reactions 3a−c. We denote the consumption rate of H_2O_2 in reaction 3b by κ (mol m^{-3} time^{-1}); stoichiometry determines the consumption rate of Ag^+ in reaction 3b to be 2κ. The consumption rate of H_2O_2 in reaction 3a per patch area is denoted by j (mol area^{-1} time^{-1}), so the production rate of Ag^+ per patch area is $2j$. Then, the flux of H_2O_2 consumed by the patch, averaged over the channel height, is j/h (mol volume^{-1} time^{-1}). Neglecting the advection of the chemical species by the flow, the height-averaged excess concentrations c_2 and c_+ satisfy a reaction−diffusion equation

$$\frac{\partial c_+}{\partial t} = D_+\nabla^2 c_+ - 2\kappa + \frac{2j}{h}\Theta(a - r) \qquad (5a)$$

$$\frac{\partial c_2}{\partial t} = D_2\nabla^2 c_- - \kappa - \frac{j}{h}\Theta(a - r) \qquad (5b)$$

where $\Theta(a - r)$ is the unity over the patch (radius a) and zero outside of it. The diffusion coefficients of Ag^+ and H_2O_2 in water are $D_+ \approx 1.6 \times 10^{-9}$ m^2 s^{-1} and $D_2 \approx 1.4 \times 10^{-9}$ m^2 s^{-1}, respectively.[29,30]

A scaling estimate of the density gradient at the edge of the patch is obtained by integrating eq 5a over the patch area. At steady state, this balance gives $\frac{\partial c_+}{\partial r} \sim -\frac{a}{hD_+}(j - h\kappa)$ and $\frac{\partial c_2}{\partial r} \sim \frac{a}{2hD_2}(j + h\kappa)$ close to the edge of the patch, where $j \geq h\kappa$ (the consumption rate of Ag^+ in the fluid cannot exceed the production rate at the patch). Thus, the Ag^+ concentration c_+ decreases away from the patch, while the H_2O_2 concentration c_2 increases away from the patch (H_2O_2 is consumed both on the patch and in the bulk). Using eq 4 to

relate species concentrations to density, the radial density gradient near the edge of the patch is then estimated as

$$\frac{\partial \rho}{\partial r}\Big|_{r=a} \sim \frac{a}{h}\left[-\frac{M_+ + M_w/2}{D_+}(j - h\kappa) + \frac{M_2 - M_w}{2D_2}\right.$$
$$\left. (j + h\kappa)\right] \qquad (6)$$

which may be either positive or negative depending on the relative values of the reaction rate κ and surface flux j. It is convenient to define the diffusivity ratio $\mathcal{D} = D_+/D_2 \approx 1.2$ and the molar mass ratio $\mathcal{M} = \frac{M_2 - M_w}{2M_+ + M_w} \approx$ 0.068. Using eq 6 with eq 2 leads to an estimate of the maximum horizontal flow speed near the edge of the patch

$$u_{max}|_{r=a} \sim \frac{gah^2(2M_+ + M_w)}{144\sqrt{3}\,\mu\,D_+}(j - h\kappa)$$
$$\left[1 - \mathcal{DM}\frac{(j + h\kappa)}{(j - h\kappa)}\right] \qquad (7)$$

Positive u_{max} indicates outward flow and negative u_{max} indicates inward flow; the flow direction depends on the relative values of j and $h\kappa$, as well as the diffusivity ratio. For the values of $\mathcal{D}$ and $\mathcal{M}$ above, eq 7 predicts outward flow if $j/(h\kappa) > 1.2$ (patch reaction is sufficiently fast) and inward flow if $1 \leq j/(h\kappa) < 1.2$; in the latter case, the density increase due to any excess Ag^+ ions produced in reaction 3a is not sufficient to offset the density decrease due to the decomposition of H_2O_2 in reaction 3b.

To estimate the decomposition rate of H_2O_2 in the presence of Ag^+ and OH^- ions, we conducted a separate experiment where a known concentration of H_2O_2 was added to a known concentration of Ag^+ ions at a prescribed pH. No patch was present, so reaction 3a does not occur, and therefore, we expect any decomposition of H_2O_2 to be solely due to reaction 3b. We monitored the concentration of H_2O_2 using UV−vis measurements (Figure S1). The concentration of H_2O_2 was found to decrease over time, which allowed us to estimate $\kappa \approx$ 0.02 mol m^{-3} min^{-1}. In our micropump experiments involving the silver patch, the H_2O_2 consumption rate at the patch (j) is more difficult to estimate since it is always accompanied by reaction 3b, which also consumes H_2O_2. However, from the species conservation arguments described above, we expect j to be on the order of $h\kappa$ close to the conditions at which the flow reverses the direction. Estimating $j \approx 2 h\kappa \approx 0.6$ μmol m^{-2} s^{-1} leads to a maximum outward flow speed of 3.5 μm s^{-1} at the edge of the patch. This order-of-magnitude estimate for the flow speed is consistent with the experimental observations (Figure 2A).

To go beyond the scaling estimates, it is necessary to consider detailed reaction kinetics to obtain streamline portraits. The main experimental features are found to be captured by modeling the patch reaction rate j as independent of the ion concentrations (catalyst-limited reaction). The bulk reaction is modeled with a rate law linear in the excess H_2O_2 present in solution, so $\kappa = kc_+$ with an effective rate constant k that has units of inverse time. Substituting this rate law into eq 5a yields

$$\frac{\partial c_+}{\partial t} = D_+\nabla^2 c_+ - 2kc_+ + \frac{2j}{h}\Theta(a - r) \qquad (8a)$$
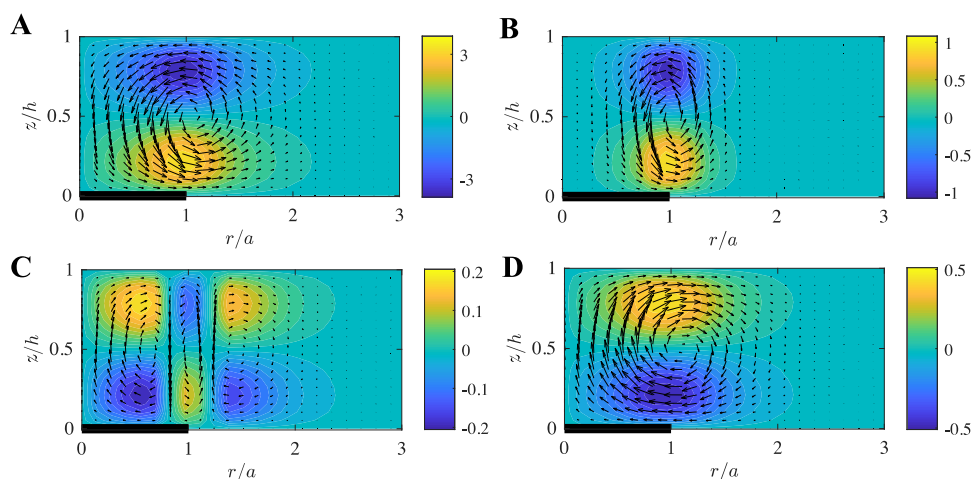
Figure 5. Sectional view showing the flow structure of the fluid next to the patch, as evaluated using the mathematical model, when (A) $\alpha = 0.5$, (B) $\alpha = 4$, (C) $\alpha = 7$, and (D) $\alpha = 20$, at time $t = 1800$ s with the patch reaction rate $j = 0.6$ μmol m^{-2} s^{-1} as estimated in the main text. Colors indicate the flow speed $|u(r,z,t)|$ in μm s^{-1}. Arrows indicate the fluid velocity $u(r,z,t)$. The patch is indicated by the thick black horizontal line at the bottom left of the plots. The flow effectively reverses the direction as α is increased from small values (silver ions are consumed very slowly) to large values (silver ions are consumed immediately after they are generated).
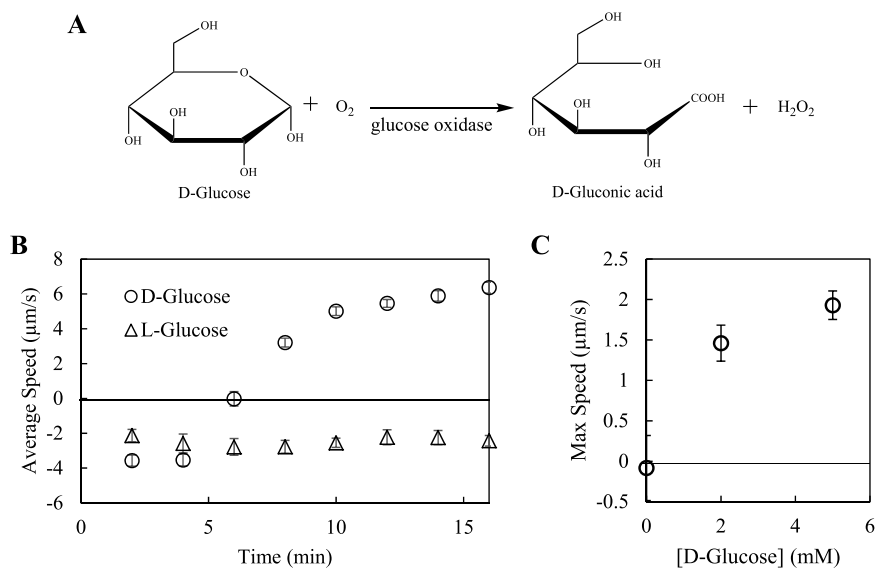
Figure 6. (A) GOx catalyzes the conversion of D-glucose to gluconic acid and H$_2$O$_2$. (B) Plot of the average fluid flow speeds versus time with 1 mg mL^{-1} GOx, 10 mM H$_2$O$_2$, and 10 mM D-glucose (circles) or 10 mM L-glucose (triangles). (C) Graph of the maximum pumping speed versus the concentration of glucose, in the absence of externally added H$_2$O$_2$ and with 1 mg mL^{-1} GOx. Negative fluid flows indicate the flow toward the silver patch (inward pumping) and positive fluid flows indicate the flow away from the silver patch (outward pumping). Error bars represent the standard deviation obtained from tracking 30 particles. The dimensions of the chamber are shown in Figure 1; the patch diameter was 5 mm.

$$\frac{\partial c_2}{\partial t} = D_2 \nabla^2 c_2 - kc_+ - \frac{j}{h}\Theta(a - r) \qquad (8b)$$

Analyzing eq 8a yields a length scale $l = \sqrt{D_+/(2k)}$, which represents the typical distance over which Ag$^+$ ions produced at the patch (in reaction 3a) are able to diffuse before being consumed in reaction 3b. The system of eq 7 can be recast such that its behavior depends on two dimensionless parameters: the diffusivity ratio $\mathcal{D} = D_+/D_2$ defined previously and the ratio of the patch radius a to the reaction−diffusion length, $\alpha = a/l = \sqrt{2k a^2/D_+}$, which is related to the consumption rate of silver ions k. The parameter α is most relevant here since the rate constant k can vary substantially depending on the pH and the buffer concentration. Also, the

characteristic time scale for the diffusion of ions across the patch, $t_d = a^2/D_+$, which, for our experimental parameters, is on the order of 2 h, is much longer than the time over which the flow is established and sustained.

We solved eq 8a for the axisymmetric flow around a circular patch (radius a) to obtain the channel height-averaged concentrations c_+ (r,t) and c_2 (r,t), which determine the density excess $\rho(r,t)$ through eq 5a and subsequently the fluid velocity field via eq 1. Numerical solutions at different values of α (with fixed $\mathcal{D} = 1.2$ and $\mathcal{M} = 0.068$) then lead to the flow portraits shown in Figure 5. For the patch reaction flux in the range estimated above ($j \approx 0.6$ μmol m^{-2} s^{-1}) and for the times relevant to the experiments ($\sim$30 min), we obtain flow speeds of a few microns per second, consistent with the experimental observations. Furthermore, as the dimensionless

ratio α (related to the reaction rate of reaction 3b) increases, we find a reversal of the flow from outward pumping (small α) to inward pumping (large α), as shown in Figure 5.

For small α, silver ions are produced in excess at the patch ($j \gg h\kappa$) and have sufficient time to diffuse away before being consumed. This establishes a density gradient with a higher density over the patch, resulting in a buoyancy-generated outward pumping. On the contrary, for large α, silver ions are consumed almost immediately after they are generated ($j \approx h\kappa$) and therefore do not affect the density. However, the simultaneous consumption of denser H_2O_2 to produce less dense water over the patch sets up a density gradient that leads to an inward flow. At intermediate values of α between 7 and 9, the flow is much slower (about 0.1 μm s^{-1}) and has a somewhat more complicated structure, which corresponds to a crossover regime between the inward and outward pumping.

Thus, our model-coupling chemical kinetics and flow rationalize the observed flow structures and speed as a consequence of buoyancy resulting from the differential transport of the reactants and products of the reaction. It should be noted that, in general, the reaction rate coefficients j and k will not be constant but vary with the concentrations of the reactants and products, as well as the details of the buffer chemistry. While this connection remains to be studied in detail, we expect the general principles applied here to remain applicable to a wide range of systems where small density differences between reactants, products, and intermediate species can result in appreciable buoyancy-driven flows.

Dynamically Changing pH Using Enzyme Catalysis. Until this point, we observed changes in the direction and speed of the flow at a fixed pH. To further probe our system, we introduced an enzyme that would lower the pH over time. To do this, we used glucose oxidase (GOx), which converts D-glucose to gluconic acid and H_2O_2 (Figure 6A).[20]

We use unbuffered water in our experimental setup, which pumps the fluid inward (toward the silver patch), in the presence of H_2O_2. However, when we add GOx and D-glucose to the system, gluconic acid is produced that lowers the pH (Figure S2) and causes the flow direction to switch from inward to outward (Figure 6 and Video SV4). We compared these results to the results from experiments using L-glucose, an enantiomer of D-glucose. L-Glucose is a very similar compound, but glucose oxidase cannot catalyze the oxidation of L-glucose. This means that gluconic acid is not produced and the pH remains high (Figure S2). Therefore, we see that the flow direction remains unchanged (Figure 6). Additionally, we found that we do not need to add H_2O_2, as the GOx reaction produces sufficient H_2O_2 to induce pumping. Interestingly, the maximum speed of pumping is dependent on the concentration of glucose in the system (Figure 6C). Thus, in principle, the system can serve as a glucose sensor since pumping can be observed at physiological concentrations of glucose (about 4−6 mM).[31,32]

SUMMARY AND CONCLUSIONS

In this paper, we demonstrated an autonomous catalytically driven microscale fluid pump and showed that the flow speed and direction can be controlled using pH. A two-step silver-catalyzed conversion of hydrogen peroxide to water and oxygen is involved. Modeling, coupling the chemistry to the induced fluid flow, supports a buoyancy-driven pumping mechanism based on differences in the density between the reactants and products, causing fluid pumping to switch

direction depending on the dominant reaction. It is also possible to dynamically change the pH in our system using appropriate enzymatic reactions, thereby allowing flow reversal *in situ*. The work opens up the possibility of using these pumps for lab-on-a-chip devices, where the speed and direction of flow can be autonomously tuned by varying the pH.

ASSOCIATED CONTENT

Ⓢ Supporting Information

The Supporting Information is available free of charge at https://pubs.acs.org/doi/10.1021/acs.langmuir.0c01240.

Decomposition of H_2O_2 over time in 50 mM borate buffer (Figure S1); pH versus time for the reaction between 1 mg mL^{-1} (6.25 μM) glucose oxidase, 10 mM D-glucose, and 10 mM L-glucose (Figure S2); calibration plot of voltage versus silver ion concentration obtained from using the silver/sulfide ion-specific electrode (Figure S3) (PDF)

Fluid pumping with 10 mM borate buffer (pH 9) and 10 mM H_2O_2 (Video SV1) (AVI)

Fluid pumping with 10 mM acetate buffer (pH 4) and 10 mM H_2O_2 (Video SV2) (AVI)

Negligible fluid pumping with 10 mM MES buffer (pH 6.5) and 10 mM H_2O_2 (Video SV3) (AVI)

Fluid pumping with 1 mg mL^{-1} (6.25 μM) glucose oxidase with 10 mM D-glucose and 10 mM hydrogen peroxide (Video SV4) (AVI)

AUTHOR INFORMATION

Corresponding Authors

Bhargav Rallabandi − *Department of Mechanical Engineering, University of California, Riverside, Riverside, California 92521, United States;* Email: bhargav@engr.ucr.edu

Howard A. Stone − *Department of Mechanical Engineering and Aerospace Engineering, Princeton University, Princeton, New Jersey 08544, United States;* ⓘ orcid.org/0000-0002-9670-0639; Email: hastone@princeton.edu

Ayusman Sen − *Department of Chemistry, Pennsylvania State University, University Park, Pennsylvania 16802, United States;* ⓘ orcid.org/0000-0002-0556-9509; Email: asen@psu.edu

Authors

Kayla Gentile − *Department of Chemistry, Pennsylvania State University, University Park, Pennsylvania 16802, United States*

Subhabrata Maiti − *Department of Chemistry, Pennsylvania State University, University Park, Pennsylvania 16802, United States;* ⓘ orcid.org/0000-0002-2554-0762

Allison Brink − *Department of Chemistry, Pennsylvania State University, University Park, Pennsylvania 16802, United States*

Complete contact information is available at:
https://pubs.acs.org/10.1021/acs.langmuir.0c01240

Notes

The authors declare no competing financial interest.

ACKNOWLEDGMENTS

■ REFERENCES

(1) Laser, D. J.; Santiago, J. G. A Review of Micropumps. *J. Micromech. Microeng.* **2004**, *14*, R35–R64.

(2) Amirouche, F.; Zhou, Y.; Johnson, T. Current Micropump Technologies and Their Biomedical Applications. *Microsyst. Technol.* **2009**, *15*, 647–666.

(3) Zhou, C.; Zhang, H.; Li, Z.; Wang, W. Chemistry Pumps: A Review of Chemically Powered Micropumps. *Lab Chip* **2016**, *16*, 1797–1811.

(4) Woias, P. Micropumps - Past, Progress and Future Prospects. *Sens. Actuators, B* **2005**, *105*, 28–38.

(5) Abhari, F.; Jaafar, H.; Md Yunus, N. A. A Comprehensive Study of Micropumps Technologies. *Int. J. Electrochem. Sci.* **2012**, *7*, 9765–9780.

(6) Sengupta, S.; Patra, D.; Ortiz-Rivera, I.; Agrawal, A.; Shklyaev, S.; Dey, K. K.; Córdova-Figueroa, U.; Mallouk, T. E.; Sen, A. Self-Powered Enzyme Micropumps. *Nat. Chem.* **2014**, *6*, 415–422.

(7) Zhao, X.; Gentile, K.; Mohajerani, F.; Sen, A. Powering Motion with Enzymes. *Acc. Chem. Res.* **2018**, *51*, 2373–2381.

(8) Farniya, A. A.; Esplandiu, M. J.; Bachtold, A. Sequential Tasks Performed by Catalytic Pumps for Colloidal Crystallization. *Langmuir* **2014**, *30*, 11841–11845.

(9) Esplandiu, M. J.; Zhang, K.; Fraxedas, J.; Sepulveda, B.; Reguera, D. Unraveling the Operational Mechanisms of Chemically Propelled Motors with Micropumps. *Acc. Chem. Res.* **2018**, *51*, 1921–1930.

(10) Farniya, A. A.; Esplandiu, M. J.; Reguera, D.; Bachtold, A. Imaging the Proton Concentration and Mapping the Spatial Distribution of the Electric Field of Catalytic Micropumps. *Phys. Rev. Lett.* **2013**, *111*, No. 168301.

(11) Kline, T. R.; Paxton, W. F.; Wang, Y.; Velegol, D.; Mallouk, T. E.; Sen, A. Catalytic Micropumps: Microscopic Convective Fluid Flow and Pattern Formation. *J. Am. Chem. Soc.* **2005**, *127*, 17150–17151.

(12) Valdez, L.; Shum, H.; Ortiz-Rivera, I.; Balazs, A. C.; Sen, A. Solutal and Thermal Buoyancy Effects in Self-Powered Phosphatase Micropumps. *Soft Matter* **2017**, *13*, 2800–2807.

(13) Kong, L.; Mayorga-Martinez, C. C.; Guan, J.; Pumera, M. Photocatalytic Micromotors Activated by UV to Visible Light for Environmental Remediation, Micropumps, Reversible Assembly, Transportation, and Biomimicry. *Small* **2019**, No. 1903179.

(14) Subramanian, S.; Catchmark, J. M. Control of Catalytically Generated Electroosmotic Fluid Flow through Surface Zeta Potential Engineering. *J. Phys. Chem. C* **2007**, *111*, 11959–11964.

(15) Solovev, A. A.; Sanchez, S.; Mei, Y.; Schmidt, O. G. Tunable Catalytic Tubular Micro-Pumps Operating at Low Concentrations of Hydrogen Peroxide. *Phys. Chem. Chem. Phys.* **2011**, *13*, 10131–10135.

(16) Alarcón-Correa, M.; Günther, J. P.; Troll, J.; Kadiri, V. M.; Bill, J.; Fischer, P.; Rothenstein, D. Self-Assembled Phage-Based Colloids for High Localized Enzymatic Activity. *ACS Nano* **2019**, *13*, 5810–5815.

(17) Ortiz-Rivera, I.; Shum, H.; Agrawal, A.; Sen, A.; Balazs, A. C. Convective Flow Reversal in Self-Powered Enzyme Micropumps. *Proc. Natl. Acad. Sci. U.S.A.* **2016**, *113*, 2585–2590.

(18) Jun, I. K.; Hess, H. A Biomimetic, Self-Pumping Membrane. *Adv. Mater.* **2010**, *22*, 4823–4825.

(19) Das, S.; Shklyaev, O. E.; Altemose, A.; Shum, H.; Ortiz-Rivera, I.; Valdez, L.; Mallouk, T. E.; Balazs, A. C.; Sen, A. Harnessing Catalytic Pumps for Directional Delivery of Microparticles in Microchambers. *Nat. Commun.* **2017**, *8*, No. 14384.

(20) Fu, L. H.; Qi, C.; Lin, J.; Huang, P. Catalytic Chemistry of Glucose Oxidase in Cancer Diagnosis and Treatment. *Chem. Soc. Rev.* **2018**, *47*, 6454–6472.

(21) Cauchy, X.; Klemberg-Sapieha, J. E.; Therriault, D. Synthesis of Highly Conductive, Uniformly Silver-Coated Carbon Nanofibers by Electroless Deposition. *ACS Appl. Mater. Interfaces* **2017**, *9*, 29010–29020.

(22) Anderson, J. L. Transport Mechanisms of Biological Colloids. *Ann. N. Y. Acad. Sci.* **1986**, *469*, 166–177.

(23) Velegol, D.; Garg, A.; Guha, R.; Kar, A.; Kumar, M. Origins of Concentration Gradients for Diffusiophoresis. *Soft Matter* **2016**, *12*, 4686–4703.

(24) Prieve, D. C.; Anderson, J. L.; Ebel, J. P.; Lowell, M. E. Motion of a Particle Generated by Chemical Gradients. Part 2. Electrolytes. *J. Fluid Mech.* **1984**, *148*, 247–269.

(25) Birikh, R. V. Thermocapillary Convection in a Horizontal Layer of Liquid. *J. Appl. Mech. Tech. Phys.* **1966**, *7*, 43–44.

(26) Selva, B.; Daubersies, L.; Salmon, J. B. Solutal Convection in Confined Geometries: Enhancement of Colloidal Transport. *Phys. Rev. Lett.* **2012**, *108*, No. 198303.

(27) Liu, Y.; Rallabandi, B.; Zhu, L.; Gupta, A.; Stone, H. A. Pattern Formation in Oil-in-Water Emulsions Exposed to a Salt Gradient. *Phys. Rev. Fluids* **2019**, *4*, No. 084307.

(28) Merkulova, N. D.; Zhutaeva, G. V.; Shumilova, N. A.; Bagotzky, V. S. Reactions of Hydrogen Peroxide on a Silver Electrode in Alkaline Solution. *Electrochim. Acta* **1973**, *18*, 169–174.

(29) *Handbook of Chemistry and Physics*, 100th ed. In Rumble, J. R., Ed.; CRC Press: Boca Raton, FL, 2019.

(30) Maiti, S.; Shklyaev, O. E.; Balazs, A. C.; Sen, A. Self-Organization of Fluids in a Multienzymatic Pump System. *Langmuir* **2019**, *35*, 3724–3732.

(31) Wang, J. Electrochemical Glucose Biosensors. *Chem. Rev.* **2008**, *108*, 814–825.

(32) Reach, G.; Wilson, G. S. Can Continuous Glucose Monitoring Be Used for the Treatment of Diabetes? *Anal. Chem.* **1992**, *64*, 381A–386A.